NJC

Accepted Manuscript

This is an *Accepted Manuscript*, which has been through the Royal Society of Chemistry peer review process and has been accepted for publication.

Accepted Manuscripts are published online shortly after acceptance, before technical editing, formatting and proof reading. Using this free service, authors can make their results available to the community, in citable form, before we publish the edited article. We will replace this *Accepted Manuscript* with the edited and formatted *Advance Article* as soon as it is available.

You can find more information about *Accepted Manuscripts* in the Information for Authors.

Please note that technical editing may introduce minor changes to the text and/or graphics, which may alter content. The journal's standard Terms & Conditions and the Ethical guidelines still apply. In no event shall the Royal Society of Chemistry be held responsible for any errors or omissions in this *Accepted Manuscript* or any consequences arising from the use of any information it contains.

ROYAL SOCIETY OF CHEMISTRY

www.rsc.org/njc

Experimental and theoretical study of intramolecular regioselective oxidations of 6-substituted 2,3-dimethylquinoxaline derivatives

Javier Peralta-Cruz, Mónica Díaz-Fernández, Alberto Ávila-Castro*
Departamento de Química Orgánica, Escuela Nacional de Ciencias Biológicas del Instituto Politécnico Nacional, Carpio y plan de Ayala S/N, Colonia Santo Tomás, 11340 Ciudad de México, México.
*David Ortegón-Reyna, Armando Ariza-Castolo**
Departamento de Química, Centro de Investigación y de Estudios Avanzados del Instituto Politécnico Nacional, Av. IPN 2508, San Pedro Zacatenco, 07360, Ciudad de México, México.

Abstract

An experimental and theoretical study of the regioselective Riley oxidation was conducted on a series of 2,3-dimethyl-6-substituted-quinoxalines bearing EWG (NO_2, CN, CF_3, Cl, Br, F, COOH, COOMe, COPh) and EDG (2,3-dimethylquinoxaline, OMe, OH, NH_2) substitutions. The nitrogen lone pair of electrons of the symmetric benzopyrazine moiety initiates the oxidation and promotes nucleophilic competition between the two active sites to give the carbaldehyde regioisomers **a** and **b**. The mesomeric effect provides the dominant contribution to the regioselectivity. The compounds were characterized by NMR, measuring the ^{1}H, ^{13}C, pfg-HSQC, pfg-HMBC, and ^{15}N, ^{1}H correlation signals established by pfg-HMQC. The nucleophilic reactivity of the nitrogen was evaluated by ^{1}H NMR titration and analyzed using Perrin linearization to determine the reactivity ratio, ΔK, of the N4 and N1 nitrogen atoms. The structures were optimized using density functional theory at the ωB97XD/6-311G++(d,p) level of theory. The highest occupied molecular orbitals modeled using the HF/6-311G++(d,p) functionals revealed an asymmetric electron density that confirmed the asymmetric nucleophilicity of the nitrogen centers. These values agreed with the experimentally measured ΔK ratios. The PM6 theoretical calculations of the heats of formation of the mesomeric forms and intermediates of (2,3-dimethyl-6-substituted-quinoxalines)-SeO_2 allowed us to identify the reaction routes that minimized energy expenditures. The regioselectivities were explained in terms of the energetic diagrams of the regioisomers. All compounds evaluated indicated a preference toward forming the regioisomer **b**, except for the derivative bearing the EDG substituent (2,3-dimethylquinoxaline) which displayed a preference for regioisomer **a**.

* Corresponding authors: jperalta@ipn.mx, aariza@cinvestav.mx

1. Introduction

Quinoxaline compounds are useful in a wide variety of applications. These compounds display biological activity and provide targets for cancer therapy[1] and antimicrobial development (against bacteria, fungi, and viruses).[2] The activity of each compound depends on the substituents and their positions on the quinoxaline rings.[3] The derivatives bearing a carbonyl group at 2-position have been extensively investigated.[4,5] The biological activities of a number of quinoxalines have been evaluated *in vitro*,[6] and some have been used in veterinarian medicine.[7,8] For these reasons, the metabolism of this type of compounds has been studied *in vivo* using mass spectrometry in different physiological fluids.[9] The metabolic routes have also been investigated,[10] in addition to their toxicities.[11] The degradation of some derivatives in acids and, neutral solutions, and under basic conditions has been reported.[12] The physical and chemical properties of the quinoxalines suggest a role as anions receptors,[13] and they can display electroluminescent activity.[14]

One of the best approaches for functionalizing quinoxalines involves the use of the Riley reaction[15] which oxidizes the methyl groups to aldehydes. This reaction was used for the first time in this compound in 1951,[16] and it has been the key approach to prepare a variety of compounds ever since.[17] Some general features of these transformations have been described by Kürti, and in many cases mixture of regioisomers have been obtained.[18] Selenium dioxide oxidations at the alpha position to form the imine group in the indole and piperidine derivatives have been described as potentially involving an ene mechanism reaction.[19]

To the best of our knowledge, this is the first report of a regioselective oxidation in 2,3-dimethyl-6-substituted-quinoxalines. The static reactivity[20] is related with the chemical equilibrium and stability of reactants and products. In this context, we estimated the heats of formation of the starting material, intermediates and products, as well as the acid constants, K_a, of the 2,3-dimethyl-6-substituted-quinoxalines to understand the nucleophilicity of nitrogen.

Theoretical calculations of this type of compounds have helped to understand the thermochemical properties,[21] and the dissociation enthalpies of the N-O bond in the 1,4-dioxide derivatives.[22,23] The reactivity and regioselectivity can be rationalized on the basis of theoretical studies.[24]

2. Experimental section

2.1. General remarks

All reagents were purchased from Sigma Aldrich. The progress of each reaction was monitored by TLC. The carboxaldehyde compounds were purified by column

chromatography using silica gel 60 0.063–0.200 mm, 60 70–230 Mesh. Melting points were determined using a Cole Parmer apparatus.

2.2. Spectroscopic characterization

The NMR spectra were recorded using VNMR 300, 500 MHz Varian (^{1}H, 300 or 500 MHz; ^{13}C, 75 or 125 MHz) and ECA-500 MHz JEOL spectrometers (^{1}H, 500 MHz; ^{13}C, 125 MHz; ^{15}N, 50 MHz). The unified scale[25] was used as a primary reference based on the ^{1}H resonance of TMS in a dilute solution (volume fraction φ < 1 %) in chloroform, $(CH_3)_4Si$ (δ ^{1}H, δ ^{13}C = 0), and neat CH_3NO_2 (δ ^{15}N for Ξ ^{15}N = 10.136767 MHz). The IR spectra were obtained using a FT-IR JASCO spectrometer. The mass spectra of the compounds were determined in high resolution using a GCmate JEOL mass spectrometer outfitted with an electronic impact (EI) detector and using a HPLC-TOF system in Bruker MicrOTOF-QII 10392 and LC-MS-TOF Agilent 6500 spectrometers.

2.3. Synthesis of 2,3-dimethyl -6-substituted-quinoxalines

Three mmol 6-R-1,2-phenylenediamines and 3 mmol 2,3-butanediones were added dropwise to a 100 mL Erlenmeyer flask. The reactions were carried out under solvent-free condition at room temperature (298 ±2 K) to obtain the 2,3-dimethyl-6-substituted-quinoxalines **1**, **2**, and **6–11**. The compounds were recrystallized in a mixture of $EtOH/H_2O$ and filtered under vacuum. The syntheses of the compounds using several methods have been reported in the literature.[26-35]

2.3.1. 2,3-Dimethylquinoxaline (1). Yellow needle-shaped crystals. Yield 94%. M.p. 362–364 K. FT-IR (ATR, cm^{-1}): 3030, 2912, 1482, 1394, 1167, 756. LC-MS-TOF in HPLC-methanol solution, m/z (%) calculated: 159.0922 (100); found: 159.0916 (100) $[M+H]^+$, empirical formula $C_{10}H_{11}N_2$. Jeol ECA-500 ^{1}H NMR ($CDCl_3$): the aromatic region consists on AA'XX' system δ = 7.95 and 7.64 ($J_{AA'}$ = 0.7, J_{AX} = 8.6, $J_{AX'}$ = 1.3, $J_{XX'}$ = 7.0, 2H, H5, H8 and 2H, H6, H7 respectively), 2.71 (s, 6H, H9, H10). ^{13}C NMR ($CDCl_3$): δ = 153.56 (C2,3), 141.15 (C4a,8a), 128.92 (C6,7), 128.39 (C5,8), 23.30 (C9,10). ^{15}N NMR ($CDCl_3$): δ = -59.2 (N1,4).

2.3.2. 2,3-Dimethyl-6-nitroquinoxaline (2). Solid powder with brown color. Yield 95%. M.p. 395–397 K. FT-IR (ATR, cm^{-1}): 3041, 2920, 1577, 1528, 1339, 1324, 823, 746. LC-MS-TOF in HPLC-methanol solution, m/z (%) calculated: 204.0773 (100); found: 204.0767 (100) $[M+H]^+$, empirical formula $C_{10}H_{10}N_3O_2$. Varian VNMR-500 ^{1}H NMR ($CDCl_3$): δ = 8.82 (s, ^{4}J = 2.4 Hz, 1H, H5), 8.38 (dd, ^{4}J = 2.4 Hz, ^{3}J = 9.1 Hz, 1H, H7), 8.05 (d, ^{3}J = 9.1 Hz, 1H, H8), 2.76 (s, 3H, H9), 2.75 (s, 3H, H10). Jeol ECA-500 ^{13}C NMR ($CDCl_3$): δ = 157.3 (C3), 156.3 (C2), 147.1 (C6), 143.7 (C8a), 139.9 (C4a), 129.9 (C8), 124.8 (C5), 122.3 (C7), 23.6 (C9), 23.3 (C10). ^{15}N NMR ($CDCl_3$): δ = -12.0 (NO_2), -54.9 (N4), -58.9 (N1).

2.3.3. 2,3-Dimethyl-6-chloroquinoxaline (6). Solid powder with brown color. Yield 95%. M.p. 359–361 K. FT-IR (ATR, cm^{-1}): 3045, 2920, 1598, 1482, 1324, 830, 717. LC-MS-

TOF in HPLC-methanol solution, m/z (%) calculated: 193.0533 (100); found: 193.0527 (100) $[M+H]^+$, empirical formula $C_{10}H_{10}N_2Cl$. Jeol ECA-500 ^1H NMR ($CDCl_3$): δ = 7.92 (d, ^4J= 2.1 Hz, 1H, H5), 7.86 (d, ^3J = 8.8 Hz, 1H, H8), 7.56 (dd, ^4J = 2.1 Hz, ^3J = 8.8 Hz, 1H, H7), 2.68 (s, 3H, H10), 2.68 (s, 3H, H9). ^{13}C NMR ($CDCl_3$): δ = 154.6 (C2), 153.8 (C3), 141.4 (C4a), 139.6 (C8a), 134.4 (C6), 129.8 (C7), 129.6 (C8), 127.4 (C5), 23.2 (C9), 23.2 (C10). ^{15}N NMR ($CDCl_3$): δ= -59.4 (N1), -60.3 (N4).

2.3.4. 2,3-Dimethyl-6-bromoquinoxaline (7). Solid powder with brown color. Yield 94 %. M.p. 355–356 K. FT-IR (ATR, cm^{-1}): 3049, 2912, 1598, 1474, 1394, 1321, 823, 699. LC-MS-TOF in HPLC-methanol solution, m/z (%) calculated: 237.0027 (100); found: 237.0022 (100) $[M+H]^+$, empirical formula $C_{10}H_{10}N_2Br$. Jeol ECA-500 ^1H NMR ($CDCl_3$): δ = 8.10 (d, ^4J = 2.1 Hz, 1H, H5), 7.79 (d, ^3J= 8.8 Hz, 1H, H8), 7.69 (dd, ^4J = 2.1 Hz, ^3J= 8.8 Hz, 1H, H7), 2.69 (s, 3H, H10), 2.67 (s, 3H, H9). ^{13}C NMR ($CDCl_3$): δ = 154.6 (C2), 154.0 (C3), 141.7 (C4a), 139.8 (C8a), 132.3 (C7), 130.8 (C5), 129.7 (C8), 122.5 (C6), 23.3 (C9), 23.3 (C10). ^{15}N NMR ($CDCl_3$): δ= -59.3 (N1), -60.2 (N4).

2.3.5. 2,3-Dimethylquinoxaline-6-carboxylic acid (8). Solid powder with brown color. Yield 97%. M.p. 398 K. FT-IR (ATR, cm^{-1}): 3045, 1701, 1624, 1328, 1237, 1163, 764. LC-MS-TOF in HPLC-methanol solution, m/z (%) calculated: 203.0821 (100); found: 203.0815 (100) $[M+H]^+$, empirical formula $C_{11}H_{11}N_2O_2$. Jeol ECA-500 ^1H NMR ($CDCl_3$): δ = 8.82 (d, ^4J = 1.8 Hz, 1H, H5), 8.33 (dd, ^4J = 1.8 Hz, ^3J= 8.5 Hz, 1H, H7), 8.07 (d, ^3J= 8.5 Hz, 1H, H8), 2.79 (s, 6H, H9), 2.79 (s, 6H, H10). (DMSO-d_6): δ = 12.5 (s, broad, 1H, COOH), 8.39 (d, ^4J = 2.1 Hz, 1H, H5), 8.10 (dd, ^4J = 2.1 Hz, ^3J= 8.8 Hz, 1H, H7), 7.95 (d, ^3J= 8.8 Hz, 1H, H8), 2.65 (s, 3H, H9), 2.64 (s, 3H, H10). ^{13}C NMR (DMSO-d_6): δ = 167.2 (C=O), 156.8 (C3), 155.8 (C2), 142.9 (C8a), 140.1 (C4a), 131.2 (C6), 130.4 (C5), 128.9 (C8), 128.6 (C7), 23.5 (C9), 23.3 (C10). ^{15}N NMR (DMSO-d_6): δ= -56.1 (N4), -58.7 (N1).

2.3.6. Methyl 2,3-dimethylquinoxaline-6-carboxylate (9). Solid powder with light pink color. Yield 94%. M.p. 362–364 K. FT-IR (ATR, cm^{-1}): 2949, 2851, 1712, 1445, 1302, 1255, 1170, 756. LC-MS-TOF in HPLC-methanol solution, m/z (%) calculated: 217.0977 (100); found: 217.0971 (100) $[M+H]^+$, empirical formula $C_{12}H_{13}N_2O_2$. Jeol ECA-500 ^1H NMR ($CDCl_3$): δ = 8.65 (d, ^4J = 1.8 Hz, 1H, H5), 8.21 (dd, ^4J = 1.8 Hz, ^3J= 8.7 Hz, 1H, H7), 7.96 (d, ^3J= 8.7 Hz, 1H, H8), 3.96 (s, 3H, OCH_3), 2.71 (s, 3H, H9), 2.71 (s, 3H, H10). ^{13}C NMR ($CDCl_3$): δ = 166.5 (C=O), 155.7 (C3), 154.7 (C2), 143.2 (C8a), 140.3 (C4a), 131.1 (C5), 130.2 (C6), 128.6 (C8), 128.5 (C7), 52.5 (OCH_3), 23.4 (C9), 23.3 (C10). ^{15}N NMR ($CDCl_3$): δ= -56.0 (N4), -59.5 (N1).

2.3.7. (2,3-dimethyl-6-quinoxalinyl)phenyl-methanone (10). Yellow solid powder as needles. Yield 98%. M.p. 380–383 K. FT-IR (ATR, cm^{-1}): 3059, 2916, 1639, 1255, 852, 724. LC-MS-TOF in HPLC-methanol solution, m/z (%) calculated: 263.1184 (100); found: 263.1179 (100) $[M+H]^+$, empirical formula $C_{17}H_{15}N_2O$. Jeol ECA-500 ^1H NMR ($CDCl_3$): δ = 8.32 (d, ^4J = 1.7 Hz, 1H, H5), 8.13 (dd, ^4J = 1.7 Hz, ^3J= 8.4 Hz, 1H, H7), 8.05 (d, ^3J= 8.4 Hz, 1H, H8), 7.83 (d, ^3J = 7.8 Hz, 2H, H_{ortho}), 7.58 (t, ^3J = 7.4 Hz, 2H, H_{para}), 7.47 (dd, ^3J =

7.8 Hz, ^3J = 7.4 Hz, 2H, H_{meta}), 2.74 (s, 3H, H9), 2.71 (s, 3H, H10). ^{13}C NMR ($CDCl_3$): δ = 195.9 (C=O), 155.8 (C3), 154.9 (C2), 143.0 (C8a), 140.1 (C4a), 137.4 (C6), 137.3 (C_{ipso}), 132.7 (C_{para}), 131.8 (C5), 130.1 (2C, C_{ortho}), 128.9 (2C, C7, C8), 128.5 (2C, C_{meta}), 23.5 (C9), 23.3 (C10). ^{15}N NMR ($CDCl_3$): δ = -56.5 (N4), -59.2 (N1).

2.3.8. 2,2',3,3'-Tetramethyl-6,6'-biquinoxaline (11). Yellow solid powder. Yield 97%. M.p. 449–452 K. FT-IR (ATR, cm^{-1}): 3055, 2916, 1489, 1390, 1328, 823. LC-MS-TOF in HPLC-methanol solution, m/z (%) calculated: 315.1610 (100); found: 315.1604 (100) $[M+H]^+$, empirical formula $C_{20}H_{19}N_4$. Jeol ECA-500 ^{1}H NMR ($CDCl_3$): δ = 8.31 (d, ^4J = 1.7 Hz, 2H, H5, H5'), 8.07 (d, ^3J = 8.4 Hz, 2H, H8, H8'), 8.04 (dd, ^4J = 1.7 Hz, ^3J = 8.4 Hz, 2H, H7, H7'), 2.75 (s, 6H, H10, H10'), 2.74 (s, 6H, H9, H9'). ^{13}C NMR ($CDCl_3$): δ = 154.3 (C2), 153.8 (C3), 141.3 (C4a), 140.7 (C8a), 140.4 (C6), 129.0 (C8), 128.4 (C7), 126.6 (C5), 23.3 (C10), 23.3 (C9). ^{15}N NMR ($CDCl_3$): δ = -59.0 (N4), -60.1 (N1).

2.4. Oxidation of 2,3-dimethyl-6-substituted-quinoxalines

In the solid phase, 1 mmol 2,3-dimethyl-6-substituted-quinoxalines and 1.3 mmol selenium dioxide were added to a 50 mL flask.[36] Subsequently, 12 mL of a 5:1 (v/v) dioxane–H_2O mixture were added, and the reactions were carried out under reflux at 362 K to yield the monoaldehyde **1a** and the mixtures of monoaldehydes **2a**–**2b**, **6a**–**6b**, **7a**–**7b**, **9a**–**9b**, and **10a**–**10b**. The organic phase was extracted in ethylacetate, dried with anhydrous sodium sulfate, and concentrated under vacuum. The products were purified by column chromatography using hexane–ethylacetate mixture (9:1) as the eluent. Only compounds **2a** and **6a** were not isolated.

2.4.1. 3-methylquinoxaline-2-carbaldehyde (1a). Yellow solid powder. Yield 56 %. M.p. 391–394 K. FT-IR (ATR, cm^{-1}): 2923, 1702, 1546, 1482, 1375, 1167, 1071, 752. LC-MS-TOF in HPLC-methanol solution, m/z (%) calculated: 172.0637; found: 172 (100) $[M]^+$,[37,38] empirical formula $C_{10}H_8N_2O$. Varian VNMR-500 ^{1}H NMR ($CDCl_3$): δ = 10.22 (s, 1H, HC=O), 8.10 (d, ^3J = 8.3 Hz, 1H, H8), 7.99 (d, ^3J = 8.3 Hz, 1H, H5), 7.82 (dt, ^4J = 1.2 Hz, ^3J = 7.5 Hz, 1H, H6), 7.73 (dt, ^4J = 1.2 Hz, ^3J = 7.5 Hz, 1H, H7), 2.95 (s, 3H, H10). ^{13}C NMR ($CDCl_3$): δ = 193.4 (HC=O), 153.0 (C3), 144.7 (C2), 142.3 (C4a), 140.2 (C8a), 132.4 (C6), 129.5 (2C, C8, C7), 128.1 (C5), 22.7(C10).

2.4.2. 3-methyl-6-nitroquinoxaline-2-carbaldehyde (2b). Solid powder with brown color. Total mixture yield 53%. M.p. 372–378 K. FT-IR (ATR, cm^{-1}): 2923, 1705, 1524, 1346, 1067, 822, 741. Varian VNMR-500 ^{1}H NMR ($CDCl_3$): δ = 10.34 (s, 1H, HC=O), 8.98 (d, ^4J = 2.4 Hz, 1H, H5), 8.57 (dd, ^3J = 9.1 Hz, ^4J = 2.4 Hz, 1H, H7), 8.38 (d, ^3J = 9.1 Hz, 1H, H8), 3.09 (s, 3H, H10). ^{13}C NMR ($CDCl_3$): δ = 193.1 (HC=O), 155.8 (C3), 144.0 (C2), 142.9 (C8a), 141.9 (C4a), 131.6 (C8), 124.9 (C7), 123.2 (C5), 23.4 (C10).

2.4.3. 7-chloro-3-methylquinoxaline-2-carbaldehyde (6a). Total mixture yield 54%. JEOL GCmate-EI direct probe, m/z (%) calculated: 206.0247 (100); found: 206.0244 (29) $[M]^+$, empirical formula $C_{10}H_7N_2OCl$. Varian VNMR-500 ^{1}H NMR ($CDCl_3$): δ = 10.27 (s,

1H, HC=O), 7.83 (d, ^4J = 2.3 Hz, 1H, H5), 7.74 (d, ^3J = 9.0 Hz, 1H, H8), 7.41 (dd, ^3J = 9.0 Hz, ^4J = 2.3 Hz, 1H, H7), 3.026 (s, 3H, H10).

2.4.4. 6-chloro-3-methylquinoxaline-2-carbaldehyde (6b). Total mixture yield 54%. M.p. 392–395 K. FT-IR (ATR, cm^{-1}): 2853, 1705, 1594, 1550, 1372, 1067, 834, 752. JEOL GCmate-EI direct probe, m/z (%) calculated: 206.0247 (100); found: 206.0244 (29) $[M]^+$, empirical formula $C_{10}H_7N_2OCl$. Varian VNMR-500 ^{1}H NMR ($CDCl_3$): δ = 10.27 (s, 1H, HC=O), 8.12 (d, ^3J = 9.0 Hz, 1H, H8), 8.06 (d, ^4J = 2.3 Hz, 1H, H5), 7.74 (dd, ^3J = 9.0 Hz, ^4J = 2.3 Hz, 1H, H7), 3.02 (s, 3H, H10). ^{13}C NMR ($CDCl_3$): δ = 193.1 (HC=O), 154.9 (C3), 145.3 (C2), 143.2 (C4a), 139.4 (C8a), 139.3 (C6), 131.4 (C7), 131.3 (C8), 127.8 (C5), 23.5 (C10).

2.4.5. 7-bromo-3-methylquinoxaline-2-carbaldehyde (7a). Solid powder with light yellow color. Total mixture yield 41%. M.p. 383–385 K. FT-IR (ATR, cm^{-1}): 3081, 3048, 2839, 1712, 1379, 845, 760. LC-MS-TOF in HPLC-methanol solution, m/z (%) calculated: 283.0082 (100), 285.0062 (97); found: 283.0074 (100), 285.0055 (97) $[M+H+CH_3OH]^+$, empirical formula $C_{11}H_{12}N_2O_2Br$. Jeol ECA-500 ^{1}H NMR ($CDCl_3$): δ = 10.26 (s, 1H, HC=O), 8.35 (dd, ^4J = 1.0 Hz, ^3J = 1.6 Hz, 1H, H6), 7.93 (d, ^3J = 1.6 Hz, 1H, H5), 7.92 (d, ^4J = 1.0 Hz, 1H, H8), 2.99 (s, 3H, H10). ^{13}C NMR ($CDCl_3$): δ = 193.7 (HC=O), 154.0 (C3), 145.7 (C2), 141.6 (C4a), 141.3 (C8a), 136.4 (C8), 132.1 (C6), 129.9 (C5), 123.9 (C7), 23.4 (C10).

2.4.6. 6-bromo-3-methylquinoxaline-2-carbaldehyde (7b). Solid powder with light yellow color. Total mixture yield 41%. M.p. 391–393 K. FT-IR (ATR, cm^{-1}): 3077, 3041, 2854, 1705, 1375, 827, 760. LC-MS-TOF in HPLC-methanol solution, m/z (%) calculated: 283.0082 (100), 285.0062 (97); found: 283.0074 (100), 285.0055 (97) $[M+H+CH_3OH]^+$, empirical formula $C_{11}H_{12}N_2O_2Br$. Jeol ECA-500 ^{1}H NMR ($CDCl_3$): δ = 10.27 (s, 1H, HC=O), 8.25 (d, ^4J = 2.1 Hz, 1H, H5), 8.04 (d, ^3J = 8.8 Hz, 1H, H8), 7.87 (dd, ^4J = 2.1 Hz, ^3J = 8.8 Hz, 1H, H7), 3.01 (s, 3H, H10). ^{13}C NMR ($CDCl_3$): δ = 193.7 (HC=O), 154.7 (C3), 145.3 (C2), 143.3 (C4a), 139.5 (C8a), 133.8 (C7), 131.2 (C8), 131.1 (C5), 127.7 (C6), 23.4 (C10).

2.4.7. Methyl 2-formyl-3-methylquinoxaline-7-carboxylate (9a). Solid powder with white color. Total mixture yield 48%. M.p. 362–364 K. FT-IR (ATR, cm^{-1}): 2949, 2851, 1712, 1445, 1302, 1255, 1170, 756. Bruker MicrOTOF-QII by ESI, m/z (%) calculated: 231.0770 (100); found: 231.0764 (100) $[M+H]^+$, empirical formula $C_{12}H_{11}N_2O_3$. Varian VNMR-300 ^{1}H NMR ($CDCl_3$): δ = 10.24 (s, 1H, HC=O), 8.77 (d, ^4J = 2.4 Hz, 1H, H5), 8.38 (dd, ^4J = 2.4 Hz, ^3J = 8.7 Hz, 1H, H7), 8.02 (d, ^3J = 8.7 Hz, 1H, H8), 4.00 (s, 3H, OCH_3) 2.99 (s, 3H, H10).

2.4.8. Methyl 2-formyl-3-methylquinoxaline-6-carboxylate (9b). Solid powder with white color. Total mixture yield 48%. M.p. 380–383 K. FT-IR (ATR, cm^{-1}): 2949, 1725, 1617, 1442, 1264, 1175, 1093, 755. Bruker MicrOTOF-QII by ESI, m/z (%) calculated: 231.0770 (100); found: 231.0764 (100) $[M+H]^+$, empirical formula $C_{12}H_{11}N_2O_3$. Varian

VNMR-300 ^{1}H NMR ($CDCl_3$): δ = 10.25 (s, 1H, HC=O), 8.65 (d, ^4J = 1.4 Hz, 1H, H5), 8.29 (dd, ^4J = 1.4 Hz, ^3J = 8.7 Hz, 1H, H7), 8.15 (d, ^3J = 8.7 Hz, 1H, H8), 4.00 (s, 3H, OCH_3) 2.99 (s, 3H, H10). ^{13}C NMR ($CDCl_3$): δ = 193.4 (HC=O), 165.6 (C=O), 154.2 (C3), 146.0 (C2), 142.2 (C4a), 141.8 (C8a), 133.5 (C6), 130.8 (C5), 129.9 (C8), 129.1 (C7), 52.7 (OCH_3), 23.1 (C10).

2.4.9. 7-benzoyl-3-methylquinoxaline-2-carbaldehyde (10a). Solid powder with beige color. Total mixture yield 56%. M.p. 362–364 K. FT-IR (ATR, cm^{-1}): 2949, 2851, 1712, 1445, 1302, 1255, 1170, 756. Bruker MicrOTOF-QII by ESI, m/z (%) calculated: 277.0977 (100); found: 277.0972 (100) $[M+H]^+$, empirical formula $C_{17}H_{13}N_2O_2$. Varian VNMR-300 ^{1}H NMR (DMSO-d_6): δ = 10.30 (s, 1H, HC=O), 8.55 (d, ^4J = 1.7 Hz, 1H, H8), 8.37 (dd, ^4J = 1.7 Hz, ^3J = 8.5 Hz, 1H, H6), 8.20 (d, ^3J = 8.7 Hz, 1H, H5), 7.89 (m, 2H, H_{ortho}), 7.67 (m, 2H, H_{para}), 7.55 (m, 2H, H_{meta}), 3.08 (s, 3H, H10).

2.4.10. 6-benzoyl-3-methylquinoxaline-2-carbaldehyde (10b). Solid powder with beige color. Total mixture yield 56%. M.p. 382–388 K. FT-IR (ATR, cm^{-1}): 2919, 1705, 1650, 1605, 1546, 1438, 1257, 1119, 750, 715. Bruker MicrOTOF-QII by ESI, m/z (%) calculated: 277.0977 (100); found: 277.0972 (100) $[M+H]^+$, empirical formula $C_{17}H_{13}N_2O_2$. Varian VNMR-300 ^{1}H NMR ($CDCl_3$): δ = 10.35 (s, 1H, HC=O), 8.42 (d, ^4J = 1.7 Hz, 1H, H5), 8.33 (d, ^3J = 8.5 Hz, 1H, H8), 8.26 (dd, ^4J = 1.8 Hz, ^3J = 8.5 Hz, 1H, H7), 7.89 (m, 2H, H_{ortho}), 7.67 (m, 2H, H_{para}), 7.55 (m, 2H, H_{meta}), 3.06 (s, 3H, H10). ^{13}C NMR ($CDCl_3$): δ = 195.3 (C=O), 193.6 (HC=O), 154.5 (C3), 146.1 (C2), 142.1 (C8a), 141.8 (C6), 140.7 (C4a), 136.5 (C_{ipso}), 133.1 (C_{para}), 131.2 (C5), 130.5 (C8), 130.1 (2C, C_{ortho}), 129.7 (C7), 128.5 (2C, C_{meta}), 23.3 (C10).

2.5. NMR spectrometric titration

In an NMR tube a solution of each one of the compounds (**1**, **2**, and **6–11**) (0.05–0.17 M) in CD_3OD (0.5–0.6 mL) was prepared, using 1,4-dioxane as an internal reference (0.5–1.0 µL, δ ^{1}H 3.53). The DCl titrant solution was prepared in 2% and 5% (v/v) concentrations from DCl/D_2O (20%) in CD_3OD. The micro pH glass electrode (reference Ag/AgCl, 3.5 x 183 mm) was calibrated using a phosphate buffered at pH 7.0, 4.0, and 10.01. The ^{1}H NMR spectra were recorded on a JEOL ECA-500 spectrometer at room temperature, 295.15 ± 1 K (22 ± 1°C). The titration and data analysis procedures were conducted according to the method of Ortegón–Reyna et al.[39] using the Henderson–Hasselbalch and Perrin equations for calculating $\boldsymbol{K_a}$, $\boldsymbol{pK_a}$, $\boldsymbol{\Delta K}$, and $\boldsymbol{\Delta pK}$, the latter two of which determine the reactivity ratio between the two nucleophilic sites, **N1** vs. **N4**. Thus, the Perrin equation may be written as follows (Equation 1):

$$\left(\delta\mathrm{H10}-\delta\mathrm{H10}^{b}\right)\left(\delta\mathrm{H9}^{e}-\delta\mathrm{H9}\right)=\Delta\boldsymbol{K}\left(\delta\mathrm{H9}-\delta\mathrm{H9}^{b}\right)\left(\delta\mathrm{H10}^{e}-\delta\mathrm{H10}\right) \qquad \textbf{[1]}$$

$$\Delta \boldsymbol{K} = \frac{\left(\delta\mathrm{H10} - \delta\mathrm{H10}^{b}\right)\left(\delta\mathrm{H9}^{e} - \delta\mathrm{H9}\right)}{\left(\delta\mathrm{H9} - \delta\mathrm{H9}^{b}\right)\left(\delta\mathrm{H10}^{e} - \delta\mathrm{H10}\right)} = \frac{\mathbf{N4}}{\mathbf{N1}} \qquad [2]$$

Here, δH9^b and δH10^b are the chemical shifts corresponding to the species present at the beginning of the titration, δH9 and δH10 are the chemical shifts observed over the course of the titration, and δH9^e and δH6^e are the chemical shifts corresponding to the species present at the end of the titration. Equation 2 gives the intramolecular reactivity ratio of the **N1** and **N4** atoms with respect to the proton chemical shifts.

2.6. Computational chemistry

The theoretical calculations were performed using the Gaussian 09 package,[40] and the molecular visualization was accomplished using the GaussView 5.0 and ChemCraft 1.7 (2013) software.[41,42] Geometry optimization was applied to 2,3-dimethyl-6-substituted-quinoxalines using the density functional theory (DFT) with the long-range corrected (LC) ωB97XD and 6-311++G(d,p) basis sets that included diffusion and polarization functions and performed better than geometry optimization.[43,44] The frontier molecular orbitals (FMO) of the compounds were described using the Hartree–Fock 6-311++G(d,p) basis set. The heats of formation of the individual intermediates obtained from the oxidation of (2,3-dimethyl-6-substituted -quinoxalines)-SeO_2 were calculated using the semiempirical PM6 level of theory to determine the energetically most favorable route.[45,46] The minimum energy was verified by calculating the vibrational frequencies for the optimized structures at the same level of theory (zero imaginary frequency).

3. Results and discussion

3.1. Preparation of 2,3-dimethyl -6-substituted -quinoxalines and their oxidation

1, **2** and **6-11** synthesized via a condensation reaction between the diamines and corresponding diketones. Subsequent oxidation to give de corresponding carbaldehydes was carried out according to the technique of Wang et al. (Scheme 1).[36]

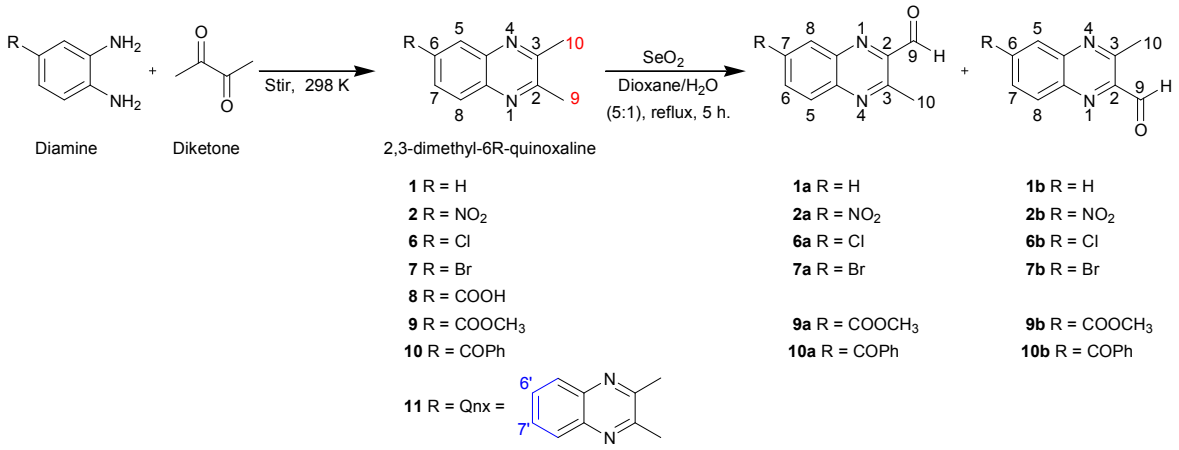

Scheme 1. Synthesis and oxidation of the 2,3-dimethyl-6-substituted-quinoxalines via condensation and the method of Wang et al.[36]

The oxidation products were the compound **1a** and a regioisomeric mixture of the monoaldehydes **2a**–**2b**, **6a**–**6b**, **7a**–**7b**, **9a**–**9b**, and **10a**–**10b**. These products were characterized by ^{1}H NMR and purified by column chromatography. The methylene group was used to calculate the ratio of regioisomers, **a**:**b**. Table 1 shows the yield and ratio of the regioisomers obtained from the oxidation of the 2,3-dimethyl-6-substituted-quinoxalines.

Table 1. Regioisomeric ratios obtained from the oxidation of each compound.

Compound	R	Total yield (%)	Regioisomer	
			a	b
1[a]	H	56	50	50
2	NO_2	53	13	87
6	Cl	54	41	59
7	Br	41	46	54
8[b]	COOH		≈44	≈56
9	COOMe	48	33	67
10	COPh	56	21	79
11[c]	Qnx		≈33	≈21

[a] Both regioisomer in compound 1 are indentical
[b] Regioisomeric ratio calculated from a linear plot of δ H9 vs. % regioisomer **b** obtained from the synthesis.
[c] A value of 46% corresponded to the regioisomer **c**. See the Supplementary Information.

The regioisomeric mixtures were readily synthesized and analyzed to obtain the product ratio. Compounds **8** and **11** were not oxidized, however; their ratio of regioisomers could be calculated using a linear regression. The chemical shift of H9 of the 2,3-dimethyl-6-substituted-quinoxalines were determined in the presence of the regioisomer **b** (Figure 1S of Supplementary Information). Compounds bearing the NO_2, $COOCH_3$, and COPh groups promoted the formation of regioisomer **b**, suggesting that **8b** (COOH), **9**, and **10** were present in a high percentage (56%). The **a**:**b** ratio for compounds **6** and **7** but different from **11**, which suggested the formation of the regioisomer **11a** (33%). These data indicates that the NO_2, $COOCH_3$, COPh, and COOH substituents strongly reduce the reactivity of the molecules. The halogens acted as weakly deactivating groups, consistent with literature reports.[47]

3.2. NMR characterization

The 2,3-dimethyl-6-substituted-quinoxalines were characterized by ^{1}H, ^{13}C, and ^{15}N NMR spectroscopy. The compounds were assigned using the pfg-HMBC and pfg-HSQC pulse sequences. The ^{15}N chemical shifts were recorded by indirectly detecting 2D heteronuclear ^{1}H–^{15}N correlations using the pfg-HMQC pulse sequence. The carboxylate and carbaldehydes were characterized by ^{1}H and ^{13}C NMR spectroscopy. The chemical shifts of the compounds are listed in the experimental section. Table 2 lists the most relevant chemical shifts of the compounds.

The carboxylates and carbaldehydes displayed characteristic ^{1}H and ^{13}C chemical shifts at 10.22–10.35 and 193.1–195.3 ppm, corresponding to H9 and C9, respectively. The chemical shifts of the other atoms in the core did not change significantly.

The chemical shifts of the 2,3-dimethyl-6-substituted-quinoxalines listed in Table 2 are related to the reactivity trend. The chemical shifts of the ^{1}H and ^{13}C methyl groups appeared at 2.67–2.79 and 23.2–23.6 ppm, respectively. The C2 and C3 shifts appeared at 153.5–157.3 ppm and were characteristic of the imine carbon of the benzopyran. The chemical shifts of the H9 and H10 depend on the substituent group. Most compounds show H9 more shifted than H10, except for compounds **6**, **7**, and **11**, which have a halogen or 2,3-dimethylquinoxaline. Moreover, the chemical shifts were a crucial role to obtain a trend in reactivity.

Table 2. Selected δ ^{1}H, δ ^{13}C, and δ ^{15}N signals from the 2,3-dimethyl-6-substituted-quinoxalines ($\Delta\delta$ in ppb), and the regioisomers **a**–**b**, obtained from oxidation in $CDCl_3$.

Compound	δ^{1}H		δ^{13}C				δ^{15}N	
	H9	H10	C2	C3	C9	C10	N1	N4
1	2.71	2.71	153.5	153.5	23.3	23.3	-59.2	-59.2
	$\Delta\delta_{H9\text{-}H10} = 0$				$\Delta\delta_{C9\text{-}C10} = 0$			
2	2.76	2.75	156.3	157.3	23.6	23.3	-58.9	-54.9
	$\Delta\delta_{H9\text{-}H10} = 3.01$				$\Delta\delta_{C9\text{-}C10} = 213$			
6	2.68	2.68	154.6	153.8	23.2	23.2	-59.4	-60.3
	$\Delta\delta_{H9\text{-}H10} = 4.25$				$\Delta\delta_{C9\text{-}C10} = 53.25$			
7	2.67	2.69	154.6	154.0	23.3	23.3	-59.3	-60.2
	$\Delta\delta_{H9\text{-}H10} = 13.4$				$\Delta\delta_{C9\text{-}C10} < \Delta\nu_{1/2} =$ 4.05 Hz			
8[a]	2.79[b]	2.79[b]	155.8	156.8	23.5	23.3	-58.7	-56.1
	$\Delta\delta_{H9\text{-}H10} < \Delta\nu_{1/2} =$ 2.82[b] Hz				$\Delta\delta_{C9\text{-}C10} = 144$			
9	2.71	2.71	154.7	155.7	23.4	23.3	-59.5	-56.0
	$\Delta\delta_{H9\text{-}H10} < \Delta\nu_{1/2} =$ 2.13 Hz				$\Delta\delta_{C9\text{-}C10} = 153$			
10	2.74	2.71	154.9	155.8	23.5	23.3	-59.2	-56.5
	$\Delta\delta_{H9\text{-}H10} = 25.4$				$\Delta\delta_{C9\text{-}C10} = 168$			
11	2.74	2.75	154.3	153.8	23.3	23.3	-60.1	-59.0
	$\Delta\delta_{H9\text{-}H10} = 4.26$				$\Delta\delta_{C9\text{-}C10} = 30.56$			
1a, 1b	10.22	2.95	144.7	153.0	193.4	22.7		
2b	10.34	3.09	144.0	155.8	193.1	23.4		
6a	10.27	3.02						
6b	10.27	3.02	145.3	154.9	193.1	23.5		
7a	10.26	2.99	145.7	154.0	193.7	23.4		
7b	10.27	3.01	145.3	154.7	193.7	23.4		
9a	10.24	2.99						
9b	10.25	2.99	146.0	154.2	193.4	23.1		
10a	10.30	3.08						
10b	10.35	3.06	146.1	154.5	195.3	23.3		

[a] Obtained in DMSO-d_6 at 500 MHz [b] Obtained in $CDCl_3$ at 500 MHz. See the Experimental Section for additional details.

These results highlight the inductive and mesomeric effects of the substituent groups, along with the magnetic susceptibility effects applied by the deuterated solvent. Taken together, these effects characterized the magnetic environment around the methyl groups and identified those sites that were susceptible to oxidation. Figure 1 shows the methyl proton shift ($\Delta\delta_{H9–H10}$) values obtained in $CDCl_3$, along with the shape of the proton signal in CD_3OD and the magnetic anisotropy around the methyl groups. The H9 protons were significantly deshielded, suggesting an electrophilic character. Proton H10 of compounds **6**,

7, and **11** displayed the greatest magnetic deshielding and, therefore, a high electrophilicity. This observation suggested that the most deshielded methyl group was also the most susceptible to oxidation. Thus, the substituent at position 6, regioselectively governed the oxidation reaction (Table 1), indicating the reactivity of the methyl group.

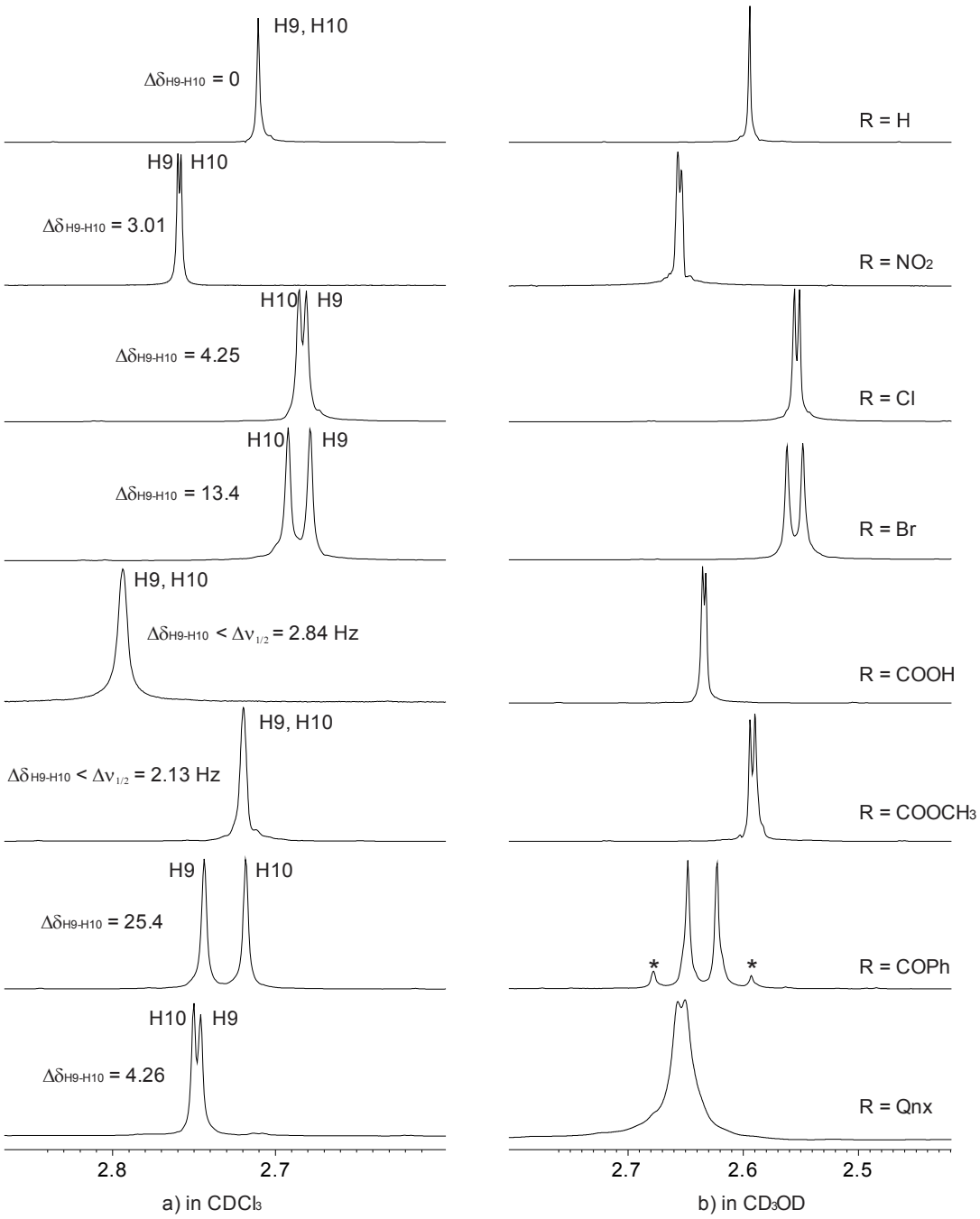

Figure 1. H9 and H10 methyl groups of the 2,3-dimethyl-6-substituted-quinoxalines in $CDCl_3$ and CD_3OD, highlighting the signal shape and magnitude in ppb of $\Delta\delta_{H9\text{-}H10}$. Note that the asterisk (*) corresponds to the side bands.

The ^{15}N chemical shifts of the N1 and N4 in the compounds are in the range of -56.0 to -60.3 ppm and were characteristic of imine derivatives. The N4 chemical shift was observed at high frequencies, unlike compounds **6** and **7**, in which the halogen substituent induced the opposite effects in terms of the frequencies of the N4 and N1 shifts (Table 2).

3.3. NMR titration analysis

A preliminary analysis of the proton and ^{15}N chemical shifts identified the reactive site; however, oxidation via the Riley oxidation[15] proceeded through a pericyclic process involving a [2,3] sigmatropic reaction in an allylic system. The first step of the oxidation involves the lone pair electrons of the imine. The [2,3] sigmatropic reaction involving the active methyl group then followed (Scheme 2). Evaluation of the reactivity of the nitrogen by ^{1}H NMR spectrometric titration was needed to verify the nucleophilicity of this center.

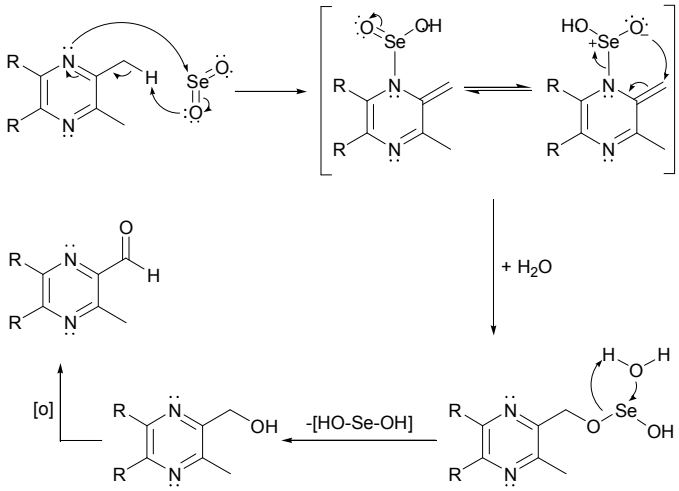

Scheme 2. Riley oxidation at the 2,3-dimethylpyrazine moiety.

The reactivities of the compounds were evaluated using deuterium chloride. The dissociation of deuterium chloride to produce deuterium (D^+) provided an electrophilic agent that attacked the nucleophilic nitrogen center. In this way, the Henderson–Hasselbalch equation was used to determine the value of ***pKa***. The reactivity ratio was determined from the **Δ*K*** values obtained using the Perrin analysis. The pH values and chemical shifts of the H9 and H10 protons during titration were determined. Table 3 shows the physicochemical parameters obtained from an analysis of the titration results.

Table 3. Physicochemical parameters obtained from NMR titration of the 2,3-dimethyl-6-

substituted-quinoxalines in CD_3OD solutions at 298 ± 1 K.

Compound		*pKa*	Δ*K*	Δ*pK**	ΔΔ*G**	Nucleophilicity N4 vs N1
1	H	0.98	1	0	0	N1 = N4
2	NO_2	0.69	0.8537	0.0686	0.3881	N1
6	Cl	0.72	1.0430	-0.0182	-0.1033	N4
7	Br	0.73	0.9983	0.0007	0.0041	N1
8	COOH	0.20	1.0146	-0.0062	-0.0355	N4
9	$COOCH_3$	0.75	1.0240	-0.0102	-0.0581	N4
10	COPh	0.54	1.0210	-0.0090	-0.0509	N4
11	Qnx	0.19	1.0325	-0.0138	-0.0784	N4

* Values were calculated with **Δ*pK*** = -log (**Δ*K***) and **ΔΔ*G*** = -RTln**Δ*K*** respectively. The nucleophilic reference value **Δ*K*** = 1 was N1 = N4; **Δ*K*** < 1 = N1; **Δ*K*** > 1 = N4.

The initial pH of the solutions of each compound fell within the range of 5.25–8.43, which corresponded to the neutral species of the 2,3-dimethyl-6-substituted-quinoxalines. Compounds **2**–**8** and **11** were more acidic than compound **1**, whereas **9** and **10** were more basic (Figure 2a). We next obtained the ***pKa*** values using the semi-logarithmic Henderson–Hasselbalch equation (Figure 2b). All compounds were more acidic than **1**, as expected. The highest acidity was obtained for the derivatives with COOH and Qnx, suggesting ready dissociation. Other compounds displayed a ***pKa*** in the range 0.54–0.75, indicating an acidity strength ordering as follows: Qnx> COOH> COPh > NO_2> Cl> Br> $COOCH_3$> H. The 2,3-dimethyl-6-substituted-quinoxalines were categorized as weak acids and displayed a trend similar to the ***pKa*** trend reported in the literature for NO_2, Cl, Br, H, and COOH substituents in aqueous solutions.[48,49]

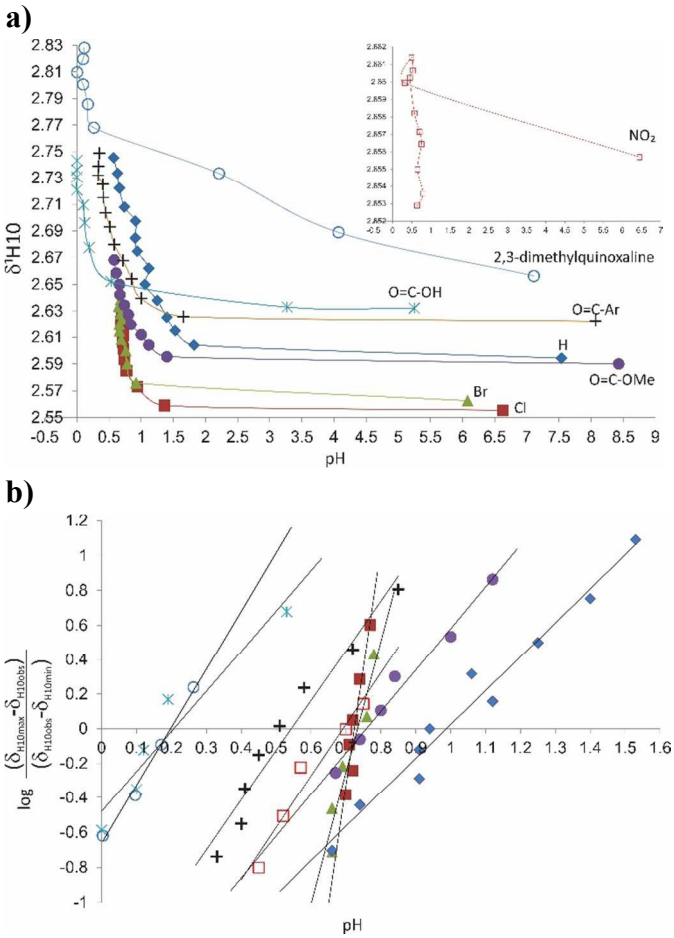

Figure 2. a) Potentiometric titration curves for the compounds **1**, **2**, **6-10**. b) Semi-logarithmic Henderson–Hasselbalch plot for each compound.

The nucleophilic reactivity of the nitrogen resulted in a $\Delta K < 1$ for compounds **2** and **7**, indicating that N1 had the largest nucleophilicity and was the first site of attack from the electrophile (by D^+). The remaining compounds yielded $\Delta K > 1$ and, both the N1 and N4 sites compete.

These results were obtained using the diagram-δ and linearization data calculated according to the Perrin analysis,[50] in which the first sign of reactivity was indicated by the correlation coefficient (R^2) of diagram-δ (Figure 3a) obtained from a plot of δH9 vs. δH10 during the spectrometric titration. The chemical shifts of H9 and H10 were linearized using the Perrin equation to calculate the ΔK value as the slope of the straight line (Table 3; Figure 3b). The relative reactivities of the nitrogen atoms could be described using equations [1] and [2], as discussed in the experimental section.

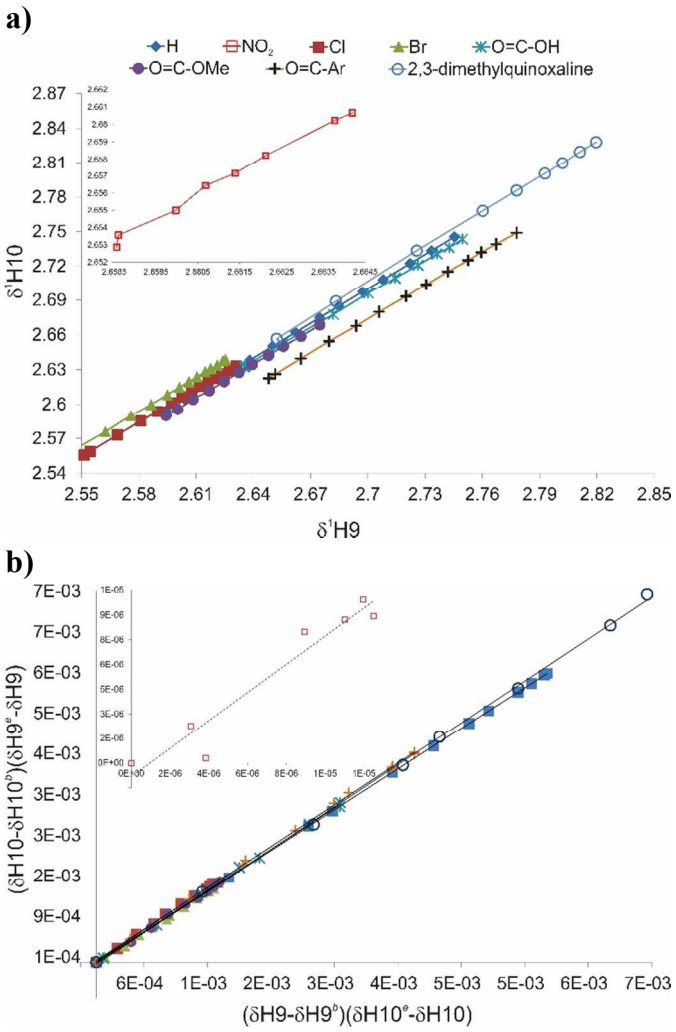

Figure 3. a) δ-diagram (δ H9 vs. δ H10), nonlinearized 2,3-dimethyl-6-substituted-quinoxalines. b) Perrin linearization plot of the data obtained from the δ-diagram.

The chemical shifts of the nitrogen yielded a qualitative trend but did not quantitatively describe the trend in the core reactivity. We therefore investigated the reactivity explicitly. The physicochemical data obtained from the spectrometric titration identified the nucleophilic sites and the primary sites of attack by an oxidizing agent in the 2,3-dimethyl-6-substituted-quinoxalines, as suggested in Scheme 2. The electron pair on the nitrogen center played an active role in initiating the Riley oxidation.

3.4. Computational chemical analysis

In order to obtain more information about the electron densities and reactivity of the 2,3-dimethyl-6-substituted-quinoxalines, the molecular structure was optimized using DFT at the ωB97XD 6-311++G(d,p) level of theory. The distribution of FMO was calculated using the Hartree–Fock 6-311++G(d,p) basis set to identify the greatest nucleophilicity by mapping the highest occupied molecular orbitals (HOMOs). The computational analysis was applied to the electron-donating groups to extend and supplement the analysis of 2,3-dimethyl-6-substituted-quinoxaline derivatives, including compounds **3–5** and **12–14** (Figure 4), which corresponded to the substituent groups CN, CF_3, F, OMe, OH, and NH_2, respectively. The syntheses of some of these structures have been reported in the literature.[2,48,51-54] These experimental data and computational analyses enabled identification of the nucleophilicities of the active sites of the compounds examined here. The theoretical calculations were used to qualitatively predict the regioselectivity of the compounds and the most favorable regioisomeric product of oxidation.

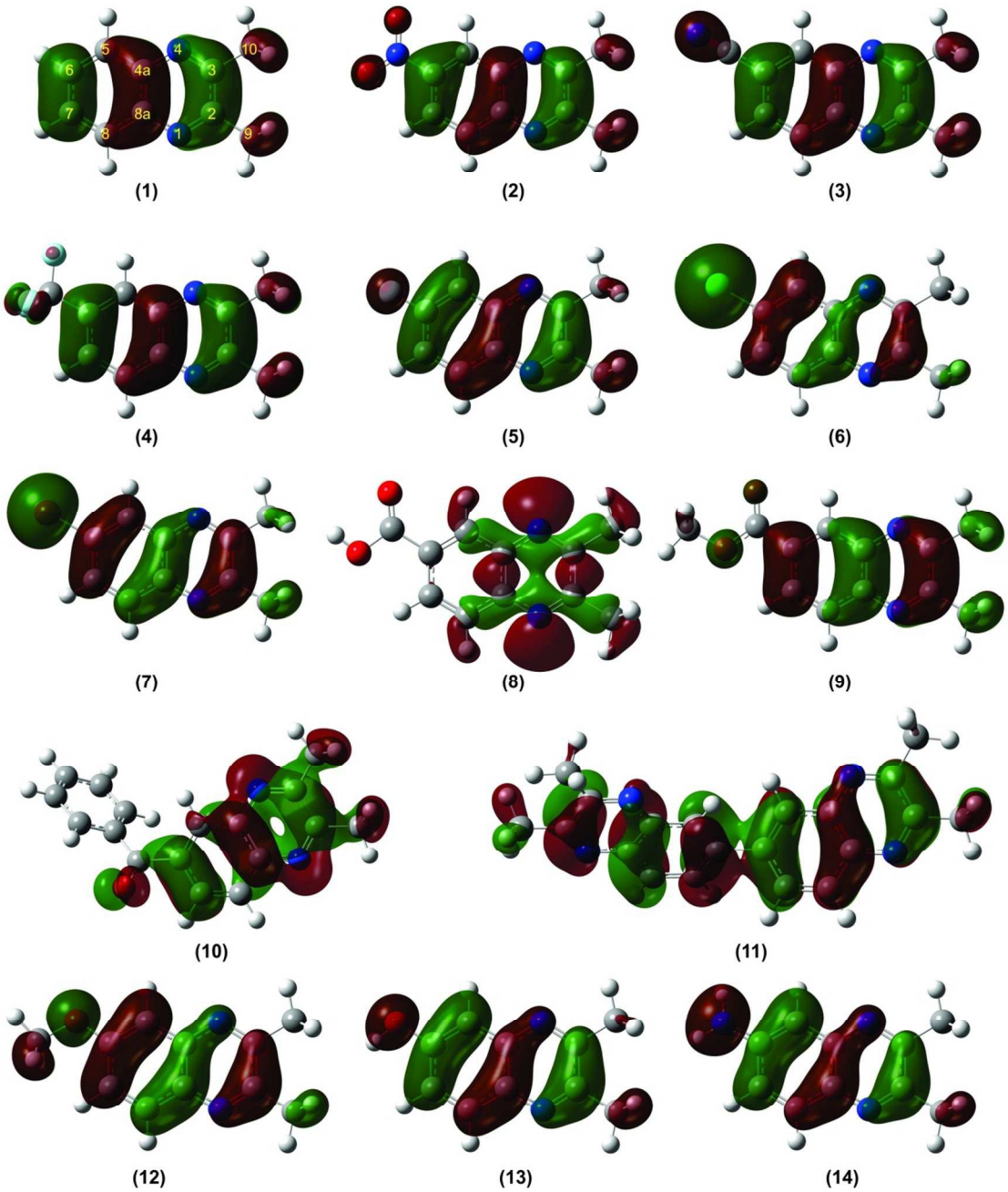

Figure 4. The HOMOs of compounds **1**–**14**, obtained at the Hartree–Fock 6-311++G(d,p) level of theory.

The optimized calculated structures of **1**, **2**, and **11** were consistent with the structures, bond distances, and angles of the X-ray structures of these compounds reported previously.[55-57] The other optimized compounds were similarly consistent with previously reported experimental results (Tables 1S and 2S of the Supplementary Information). The electrons in benzopyrazine were predicted to be delocalized across the entire system. The EDG and EWG moderately affected the symmetry and bond distances of the compounds.

The C5-C6 and C7-C8 bond distances were more characteristic of a double bond than a single bond. These results suggested that the electron density distributions across the compounds were asymmetric. This asymmetry should be reflected in the nucleophilicity of the nitrogen atoms and the electrophilicity of the methyl group. The surfaces of the HOMOs in the optimized structures displayed this characteristic asymmetry, as shown in the high-energy HOMOs plotted in Figure 4.

The substituent attached to the 2,3-dimethyl-6-substituted -quinoxaline determined the shape and distribution of the HOMOs. The C6-C7, C8-C8a-C4a, and N1-C2-C3 units in compounds **2**, **3**, **4**, and **9** differed predominantly in three electron density regions. The electron density around C6-C7 displayed a pulling effect on the EWG, resulting in a higher electron density at N1 than at N4. The chemical shift of N4 appeared at higher frequencies compared to the chemical shift of N1 due to the remote deshielding of the EWG. The electron density was higher in fragment C5-C6-C7, C8-C8a-C4a-N4, and N1-C2-C3 of **5**–**7** and **12**–**14**. The EDG exerted a pushing effect in the C5-C6-C7 region. The presence of chloro substituents and the EDG produced the opposite effect. The electron density of N4 was greater than that of N1. The experimental chemical shifts of N1 in compound **6** appeared at a high frequency, suggesting that the N1 position in compounds **12**–**14** were shifted toward higher frequencies than the N4 position. Compounds **7** and **5** displayed equivalent electron densities. The majority of the electron density was centered at N1. The shape and distribution of the electron density in compound **11** were characteristic of the compounds with EDG. The density and electronic deshielding at the N4 position were low, and the corresponding ^{15}N chemical shift appeared at high frequencies. This correlation was not as striking in the HOMOs of compounds **8** and **10**, due to their similarities to compound **9**. Experimentally, **8**, **9**, and **10** displayed similar ^{15}N chemical shifts. A similar analysis of the methyl groups allowed us to visualize the correlation between the electron density and the $\Delta\delta_{H9–H10}$, where the presence of the substituent R in 2,3-dimethyl-6-substituted-quinoxaline resulted in mesomeric inductive effects on the methyl groups. The absence of electron density at the methyl group suggested greater electronic deshielding, a high electrophilicity, and a shift in the ^{1}H or ^{13}C peak positions toward higher frequencies. A higher electron density suggested the opposite effect. The magnitudes of the HOMO densities around the methyl groups in the 2,3-dimethyl-6-substituted-quinoxalines (Figure 4) **5**–**7** and **11**–**14** were remarkably different. Compounds **2**–**4** displayed more moderate differences. Compounds **8** and **9** displayed a weak difference ($\Delta\delta_{H9\text{-}H10} \leq \Delta\nu_{1/2}$). These differences were correlated with the $\Delta\delta_{H9\text{-}H10}$ and the observed ^{1}H NMR spectra, suggesting the presence of anisotropic magnetic environments around the methyl groups. The electron densities around the methyl groups in compound **10** were equivalent, based on the HOMO density. Experimentally, these methyl groups differed by $\Delta\delta_{H9\text{-}H10}$ = 25.4 ppb due to the field effect of the COPh substituent on the methyl group.

The HOMO revealed that the nitrogen atom was more nucleophilic than the first site of electrophile attack. The experimental data obtained from the ΔK values calculated from the spectrometric titration data were self-consistent. The compounds bearing NO_2 and Br substituents displayed a high electronic density at N1, consistent with a $\Delta K < 1$. These results suggested that compounds **3**, **4**, and **5** yielded equal ΔK values. Compounds **6** and **9–11** revealed a high nucleophilicity at N4, with a $\Delta K > 1$. Compounds **12–14** appeared to be characterized by $\Delta K > 1$ due to the high electronic density at N4. The theoretical results and experimental data were crucial for predicting the reactivities and the initial Riley oxidation reaction sites on the benzopyrazine systems examined here.

With knowledge of the initial reaction site on the 2,3-dimethyl-6-substituted-quinoxalines, we proposed an extension of the Riley oxidation mechanism (Scheme 2) of 2,3-dimethyl-6-substituted-quinoxalines. The presence of a substituent on the quinoxaline core affects the regioselectivity of the methyl oxidation product exerting the strongest influence on the most nucleophilic nitrogen center, which is the initial site of attack. The oxidation mechanism proceeded along the path with the lowest barrier. If the initial attack occurred at the N1 site, oxidation continued to the methyl C9 to yield the desired regioisomer. If the attack instead occurred at N4, oxidation proceeded at the methyl C10 (Scheme 3). In this case, both of the nucleophilic sites competed for oxidation. Compounds **2** and **7**, which bear NO_2 and Br groups, selectively tuned the nucleophilicity of N1 to favor regioselective oxidation at the methyl C9. These effects favored the formation of regioisomer **b**, suggesting that CN, CF_3, and F provided equivalent regioselectivities. The opposite effect was observed using the Qnx substituent in compound **11**. In this case, the N4 center was the most nucleophilic, and oxidation proceeded at the methyl C10 to form the regioisomer **a**.

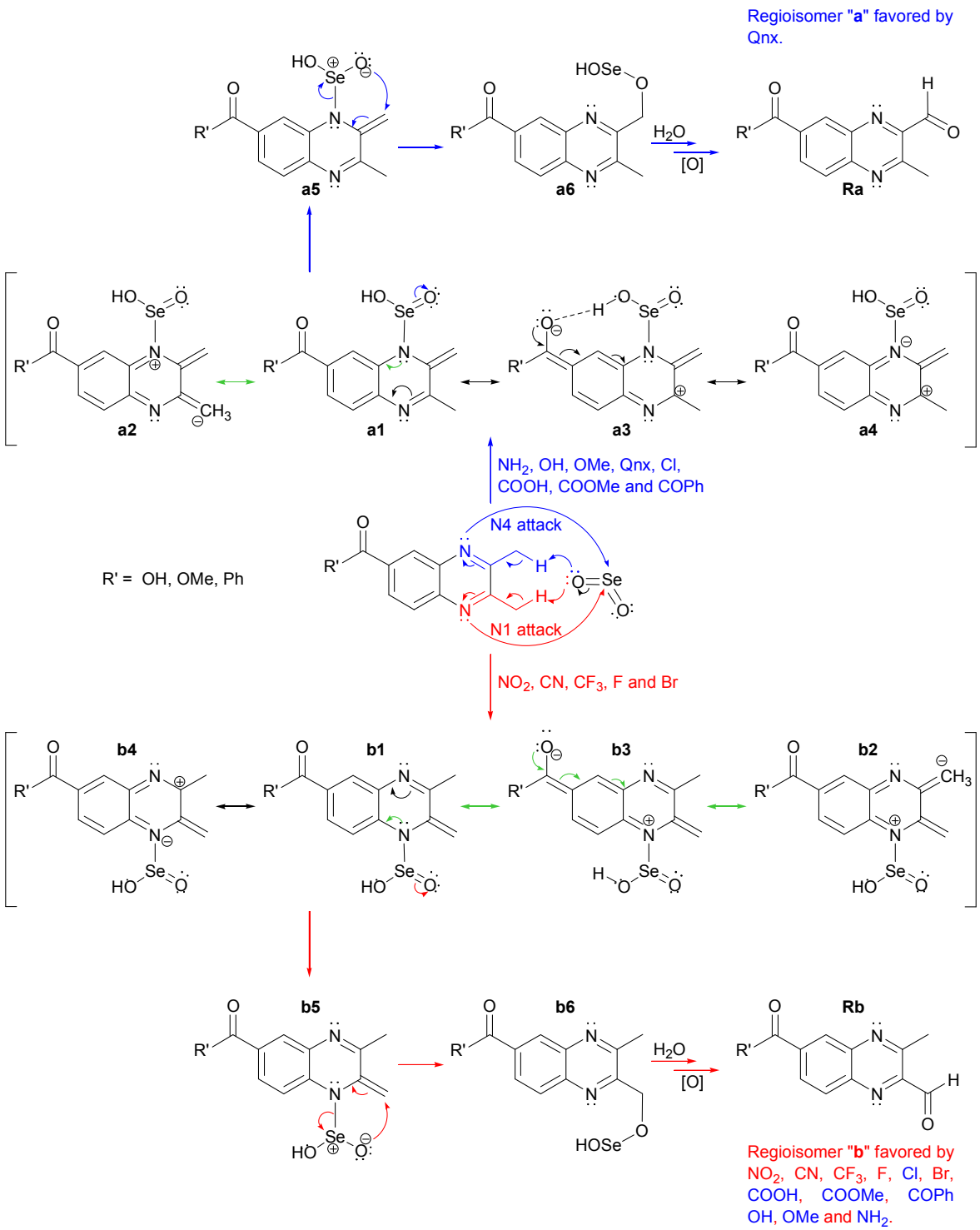

Scheme 3. Alternative mechanism of 2,3-dimethyl-6-substituted-quinoxaline oxidation, indicating the initial nucleophilic attack and the formation of the major regioisomer as a result of the EWG and EDG substituent effects.

The most nucleophilic nitrogen centers associated with the chloro, carbonyl, and EDG in compounds **6**, **8–10**, and **12–14** initiated the reaction but there are other factors that determine the lack of regioselectivity. The regioselectivity appeared to depend on the substituents, suggesting that the reaction intermediates played a role. In the absence of a correlation between the strongest nucleophilic site and the major regioisomeric product, as was observed previously in the semiempirical calculations using PM6,[45] it was necessary to consider the energetics of the reaction pathways available to the intermediates and their mesomeric structures. Table 4 lists the formation energies of the principal mesomeric forms of compounds **1–14**. Scheme 3 illustrates an extended oxidation mechanism.

Table 4. Energy of formation (k*J*mol^{-1}) of the mesomeric forms of the (2,3-dimethyl-6-subtituted-quinoxaline)-SeO_2 complex through the energetic route.

Comp.	Mesomeric forms regioisomer "a"					Mesomeric forms regioisomer "b"				
	a1	**a2**	**a3**	**a4**	$A_{\Delta E}$[a]	**b1**	**b2**	**b3**	**b4**	$A_{\Delta E}$[a]
1	123.7	328.1	303.6	293.6	83	123.7	328.15	303.60	293.67	83
2	114.0	316.1	284.0	282.9	82	121.88	303.19	237.69	251.63	76
3	259.5	462.6	467.1	428.6	85	275.34	456.95	438.01	404.82	67
4	-544.9	-339.5	-285.2	-371.3	111	-532.78	-349.25	-324.18	-398.96	90
5	-76.2	124.3	295.2	90.5	167	-50.33	133.95	299.00	80.27	160
6	83.7	284.3	283.8	250.2	82	104.61	287.31	268.23	233.68	77
7	135.2	338.5	340.1	304.8	84	153.37	337.22	316.68	284.16	67
8	-133.5	0.02	69.2	-59.9	84	-130.52	-34.96	-12.72	-87.73	54
9	-212.3	-10.9	5.4	-44.1	91	-203.8	-20.46	-86.80	-72.04	44
10	114.2	315.8	331.9	281.0	89	123.56	308.62	242.97	255.54	45
11	350.1	719.9	628.3	633.4	150	370.56	722.00	559.49	654.16	192
12	-45.6	154.1	120.6	117.8	81	-14.25	168.11	124.08	112.53	77
13	-65.9	135.1	76.8	99.5	92	-33.03	150.01	80.73	94.80	84
14	112.2	317.8	252.3	280.9	98	144.19	336.58	270.03	279.44	86

[a] The value of Δ energy ($\mathbf{A_{\Delta E}}$) was calculated as the average of ΔE values obtained from the mesomeric forms (see the Supplementary Information).

During the initial stages of oxidation, the nucleophilic sites N1 and N4 competed in oxidizing the methyl group. The complex formed between selenium dioxide and the 2,3-dimethyl-6-subtituted -quinoxalines was capable of oxidizing along either of two paths. The mesomeric species led regioselectively to oxidation at the methyl via a reaction route characterized by low energy expenditure. The theoretical analysis of the compounds predicted that the regioisomer **b** would be favored. Compound **11** was predicted to favor regioisomer **a**, consistent with the experimental results listed in Table 1. The average energy ($A_{\Delta E}$) was calculated for the reaction pathway that led to the mesomeric forms (Table 4). The energy diagram for compound **8**, which bear COOH substituents, is shown in Figure 5.

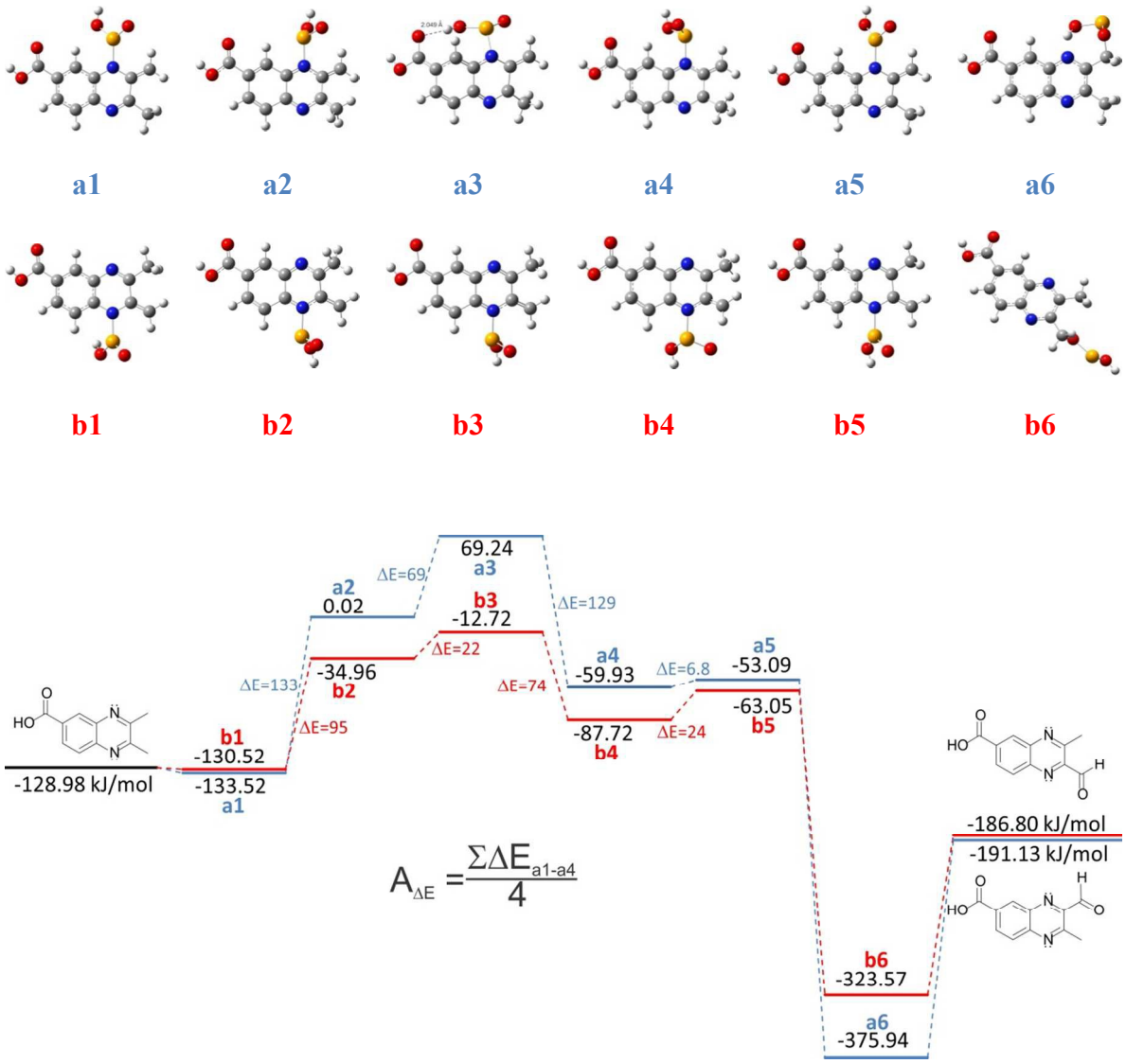

Figure 5. Energy diagrams of the regioisomers **8a** and **8b** bearing COOH group substitutions. The routes associated with the highest and lowest energy expenditures are shown.

Compound **8**, which included a COOH substituent, displayed a nucleophilic N4. Among the oxidation routes available, the favored route minimized the energy expenditure to yield regioselectively **8b**. The same result was observed for **9** and **10**. The compounds bearing Cl, OMe, OH, and NH_2 groups displayed a nucleophilic N4 and therefore energetically favored the regioisomers **b** (the energy diagram is described in detail in the Supplementary Information). These results suggested that the mesomeric effects played an important role in regioselectivity. The COOH, COOMe, COPh, OMe, OH, and NH_2 groups provided a mesomeric effect that dominated the inductive effect. By contrast, the halogenated compounds only displayed an inductive effect. Finally it should be noted that the

experimental results agreed with the theoretical analysis. Derivatives of the 2,3-dimethyl-6-subtituted-quinoxalines benefit from an analysis of the HOMO energy and the energetic route to preliminarily determine regioselectivity during a methyl Riley oxidation.

4. Conclusion

We determined the regioselectivity of the methyl oxidation reaction in 2,3-dimethyl-6-subtituted-quinoxalines. The regioselectivity effects were directed by the electron-withdrawing and electron-donating substituent groups. The experimentally determined ΔK equilibrium values obtained from the δ-diagram, the Perrin linearization, and the theoretical results indicated that the electron-withdrawing and electron-donating groups affected and directed the nucleophilicity toward the nitrogen atoms, thereby involving these centers during initiation. An extension of the mechanism underlying the Riley oxidation of this type of system was proposed. Despite behaving as activating and deactivating groups within the system, the regioselectivity directed by the electron-withdrawing and electron-donating groups was governed more by the mesomeric effects across the 2,3-dimethyl-6-substituted-quinoxaline system.

5. Acknowledgements

D. O.-R. would like to express gratitude to CONACyT for providing postdoctoral research support. J. P.-C. thanks SIP-IPN for financial support 20144003. M D.-F. thanks CONACyT for a master scholarship.

6. References

1. C. W. Lindsley, Z. Zhao, W. H. Leister, R. G. Robinson, S. F. Barnett, D. Defeo-Jones, R. E. Jones, G. D. Hartman, J. R. Huff, H. E. Huber and M. E. Duggan, *Bioorg. Med. Chem. Lett.*, 2005, **15**, 761-764.
2. A. Go, G. Lee, J. Kim, S. Bae, B. M. Lee and B. H. Kim, *Tetrahedron*, 2015, **71**, 1215-1226.
3. A. Gazit, H. App, G. McMahon, J. Chen, A. Levitzki and F. D. Bohmer, *J. Med. Chem.*, 1996, **39**, 2170-2177.
4. Y. B. Kim, Y. H. Kim, J. Y. Park and S. K. Kim, *Bioorg. Med. Chem. Lett.*, 2004, **14**, 541-544 and reference here cited.
5. M. L. Edwards, R. E. Bambury and H. W. Ritter, *J. Med. Chem.*, 1975, **18**, 637-639.
6. A. Jaso, B. Zarranz, I. Aldana and A. Monge, *J. Med. Chem.*, 2005, **48**, 2019-2025.
7. J. Zhang, Q. Peng, S. Zhang, Y. Li, S. Li, H. Gao and Z. Zhou, *J. Mol. Struct.,* 2011, **987**, 34-39.
8. ZY. Liu, LL Huang, DM Chen and ZH Yuan, *Rapid Comm. Mass Spectrom.,* 2010, **24**, 909-918.

9. Q. Shan, Y. Liu, L. He, H. Ding, X. Huang, F. Yang, Y. Li and Z. Zeng, *J. Chromatogr. B.*, 2012, **881–882**, 96-106.
10. Z. Y. Liu, L. L. Huang, D. M. Chen, M. H. Dai, Y. F. Tao, Y. L. Wang and Z. H. Yuan, *Anal. Bioanal. Chem.*, 2010, **396**, 1259-1271.
11. X. Wang, X. J. Huang, A. Ihsan, Z. Y. Liu, L. L. Huang, H. H. Zhang, H. F. Zhang, W. Zhou, Q. Liu, X. J. Xue and Z. H. Yuan, *Toxicology*, 2011, **280**, 126-134.
12. Z. Y. Liu, H. H. Zhang, X. J. Chen, X. N. Zhou, L. Wan and Z. L. Sun, *Int. J. Mass Spectrom.*, 2011, **303**, 90-96.
13. J. L. Sessler, H. Maeda, T. Mizuno, V. M. Lynch and H. Furuta, *Chem. Commun.*, 2002, 862-863.
14. S. Dailey, W. J. Feast, R. J. Peace, I. C. Sage, S. Till and E. L. Wood, *J. Mater. Chem.*, 2001, **11**, 2238-2243.
15. H. L. Riley, J. F. Morley and N. A. C. Friend, *J. Chem. Soc. (Resumed)*, 1932, 1875-1883.
16. M. Seyhan, *Chem. Ber.*, 1951, **84**, 477-477.
17. E. J. Moriconi and A. J. Fritsch, *J. Org. Chem.*, 1965, **30**, 1542-1547.
18. L. Kürti and B. Czakó, *Strategic applications of named reactions in organic synthesis*, Elsevier Academic Press, Amsterdam, 2005.
19. M. Cain, O. Campos, F. Guzman and J. M. Cook, *J. Am. Chem. Soc.*, 1983, **105**, 907-913.
20. C. L. Perrin, in *Encyclopedia of Physical Science and Technology*, Academic Press, San Diego, CA, 2002, pp. 211-243.
21. M.A.V. Ribeiro da Silva, V. M. F. Morais, M. A. R. Matos, C. M. A. Rio, C. M. G. S. Piedade, *Struct. Chem.*, 1996, **7**, 329-336
22. W. E. Acree, Jr., Joyce R. Powell, Sheryl A. Tucker, Maria D. M. C. Ribeiro da Silva, M. Agostinha R. Matos, J. M. Goncüalves, L. M. N. B. F. Santos, V. M. F. Morais, G. Pilcher, *J. Org. Chem*., 1997, **62**, 3722-3726
23. M. D. M. C. Ribeiro da Silva, J. R. B. Gomes, J. M. Goncüalves, E. A. Sousa, S. Pandey, W. E. Acree, Jr., *J. Org. Chem.*, 2004, **69**, 2785-2792
24. P. Geerlings, F. De Proft, W. Langenaeker, *Chem. Rev.* 2003, **103**, 1793-1873
25. R. K. Harris, E. D. Becker, S. M. Cabral de Menezes, R. Goodfellow and P. Granger, *Magn. Reson. Chem.*, 2002, **40**, 489-505.
26. C. Pérez-Melero, A. B. S. Maya, B. del Rey, R. Peláez, E. Caballero and M. Medarde, *Bioorg. Med. Chem. Lett.*, 2004, **14**, 3771-3774.
27. H. R. Darabi, K. Aghapoor, F. Mohsenzadeh, F. Taala, N. Asadollahnejad and A. Badiei, *Catal. Lett.*, 2009, 84-89.
28. X. Z. Zhang, J. X. Wang, Y. J. Sun and H. W. Zhan, *Chin. Chem. Lett.*, 2010, **21**, 395-398.
29. M. Hosseini-Sarvari, *J. Iran. Chem. Soc.*, 2012, **9**, 535-543.
30. J. J. Morales-Castellanos, K. Ramírez-Hernández, N. S. Gómez-Flores, O. R. Rodas-Suárez and J. Peralta-Cruz, *Molecules*, 2012, **17**, 5164.
31. A. V. Narsaiah and J. K. Kumar, *Synth. Commun.*, 2012, **42**, 883-892.
32. F. Hakimi and B. B. F. Mirjalili, *Curr. Chem. Lett.*, 2013, **2**, 105-108.
33. W. J. Zhou, X. Z. Zhang, X. B. Sun, B. Wang, J. X. Wang and L. Bai, *Russ. Chem. Bull.*, 2013, **62**, 1244-1247.
34. R. Ghorbani-Vaghei and S. Hajinazari, *J. Chem. Sci.*, 2013, **125**, 353-358.
35. A. Dwivedi, A. Singh and A. Mishra, *Chem. Sci. Trans.*, 2014, **3**, 465-469.

36. Q. Wang, S. Zhang, F. Guo, B. Zhang, P. Hu and Z. Wang, *J. Org. Chem.*, 2012, **77**, 11161-11166.
37. J. Beck, F. Ledl and T. Severin, *Carbohydr. Res.*, 1988, **177**, 240-243.
38. M. Kepez, *Monatsh. Chem.*, 1989, **120**, 127-130.
39. D. Ortegón-Reyna, C. Garcías-Morales, I. Padilla-Martínez, E. García-Báez, A. Aríza-Castolo, A. Peraza-Campos and F. Martínez-Martínez, *Molecules*, 2013, **19**, 459-481 and reference here cited.
40. M. J. Frisch, G. W. Trucks, H. B. Schlegel, G. E. Scuseria, M. A. Robb, J. R. Cheeseman, G. Scalmani, V. Barone, B. Mennucci, G. A. Petersson, H. Nakatsuji, M. Caricato, X. Li, H. P. Hratchian, A. F. Izmaylov, J. Bloino, G. Zheng, J. L. Sonnenberg, M. Hada, M. Ehara, K. Toyota, R. Fukuda, J. Hasegawa, M. Ishida, T. Nakajima, Y. Honda, O. Kitao, H. Nakai, T. Vreven, J. A. Montgomery, Jr., J. E. Peralta, F. Ogliaro, M. Bearpark, J. J. Heyd, E. Brothers, K. N. Kudin, V. N. Staroverov, R. Kobayashi, J. Normand, K. Raghavachari, A. Rendell, J. C. Burant, S. S. Iyengar, J. Tomasi, M. Cossi, N. Rega, M. J. Millam, M. Klene, J. E. Knox, J. B. Cross, V. Bakken, C. Adamo, J. Jaramillo, R. Gomperts, R. E. Stratmann, O. Yazyev, A. J. Austin, R. Cammi, C. Pomelli, J. W. Ochterski, R. L. Martin, K. Morokuma, V. G. Zakrzewski, G. A. Voth, P. Salvador, J. J. Dannenberg, S. Dapprich, A. D. Daniels, O. Farkas, J. B. Foresman, J. V. Ortiz, J. Cioslowski and D. J. Fox. GAUSSIAN 09 (Revision D.01), *Gaussian, Inc*., Wallingford, CT, 2009.
41. G. A. Andrienko, CHEMCRAFT, Version 1.7 (Build 382), *Bluesnap, Inc*., Waltham, Massachusetts, 2013.
42. R. Dennington, T. Keith and J. Millam, GAUSSVIEW, Version 5.0.9, *Semichem Inc*, Shawnee Mission, KS, 2009.
43. J. D. Chai and M. Head-Gordon, *J. Chem. Phys.*, 2008, **128**, 084106.
44. J. D. Chai and M. Head-Gordon, *Phys. Chem. Chem. Phys.*, 2008, **10**, 6615-6620.
45. Y. Y. Wu, F. Q. Zhao and X. H. Ju, *J. Mex. Chem. Soc.*, 2014, **58**, 223-229.
46. SPARTAN '08, *Wavefunction, Inc*., 18401 Von Karman Ave., Suite 370 Irvine, CA 92612, 2009.
47. F. A. Carey and R. J. Sundberg, *Advanced Organic Chemistry, Part A: Structure and Mechanism*, Springer link, Charlottesville, Virginia, 2007.
48. P. Vetešník, J. Kaválek, V. Beránek and O. Exner, *Collect. Czech. Chem. Commun.*, 1968, **33**, 566-576.
49. J. H. Markgraf, R. A. Blatchly, B. M. Peake and A. S. Huffadine, *J. Chem. Eng. Data*, 1982, **27**, 473-474.
50. C. L. Perrin and M. A. Fabian, *Anal. Chem.*, 1996, **68**, 2127-2134.
51. H. Gilman and H. S. Broadbent, *J. Am. Chem. Soc.*, 1948, **70**, 2619-2621.
52. J. Jan, G. Hagen and R. Lenoir, *U. S. Patent*, 4202698.
53. S. Ajaikumar and A. Pandurangan, *Appl. Catal., A*, 2009, 184-192.
54. F. Xie, M. Zhang, H. Jiang, M. Chen, W. Lv, A. Zheng and X. Jian, *Green Chem.*, 2015, **17**, 279-284.
55. K. Wozniak, T. M. Krygowski, B. Kariuki and W. Jones, *Acta Crystallogr. Sect. C*, 1990, **46**, 1946-1947.
56. R. N. Salvatore, J. P. Kass, R. J. P. Gibson, C. H. Zambrano, R. D. Pike and E. E. Dueno, *Acta Crystallogr. Sect. E*, 2006, **62**, o4547-o4548.

57. R. M. Ghalib, R. Hashim, S. H. Mehdi, J. H. Goh and H.-K. Fun, *Acta Crystallogr. Sect. E*, 2010, **66**, o1830-o1831.

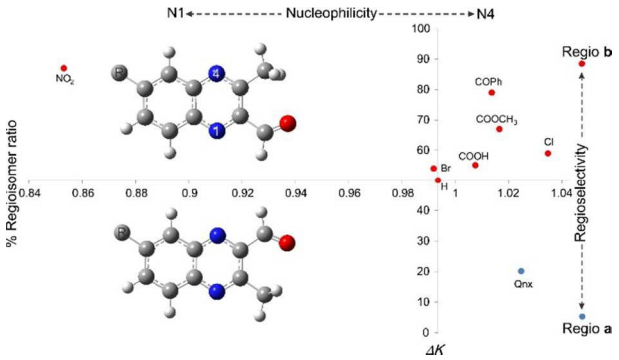

The long-range substituent effects in the Riley reaction mechanism were determined by NMR and DFT calculation.